Synthesis of ZrC_x with Controlled Carbon Stoichiometry by Low Temperature Solid State Reaction

Yue Zhou*, Thomas W. Heitmann', William G. Fahrenholtz*, Gregory E. Hilmas*

*Department of Materials Science and Engineering, Missouri University of Science and Technology, Rolla, Missouri 65409, USA

' The Missouri Research Reactor, University of Missouri, Columbia, Missouri 65211, USA

Abstract:

Zirconium carbide (ZrC_x) powders were synthesized at temperatures between 1300°C and 2000°C by solid state reaction of zirconium hydride (ZrH₂) and carbon black. Crystal structure, lattice parameters, and grain sizes of the as-synthesized ZrC_x powders were characterized for two different starting ZrH₂:C ratios of 1:0.60 and 1:0.98. Powders with stoichiometry approaching ZrC_{0.98} were synthesized at temperatures as low as 1600°C whereas ZrC_x powders synthesized at lower temperatures had lower carbon contents regardless of the starting ZrH₂:C ratio. Crystallite sizes as small as about 50 nm were obtained due to the low synthesis temperature. Oxygen dissolved into the ZrC_x lattice when carbon vacancies were present. Neutron diffraction analysis was used to determine that carbon stoichiometry increased and dissolved oxygen content decreased as synthesis temperature increased.

Keywords: Zirconium carbide powder; Low temperature synthesis; X-ray diffraction; Carbon stoichiometry; Powder oxidation; Electron microscopy; Neutron diffraction; Intrinsic property.

Corresponding author: William G. Fahrenholtz Tel.: +1 573-341-6343. *E-mail address:* billf@mst.edu. Department of Materials Science and Engineering, Missouri University of Science and Technology, Rolla, Missouri 65409, USA

Yue Zhou Tel.: +1 (304)777-8907. *E-mail address*: yznwb@mst.edu. Department of Materials Science and Engineering, Missouri University of Science and Technology, Rolla, Missouri 65409, USA

Gregory E. Hilmas Tel.: +1 573-341-6102. *E-mail address:* ghilmas@mst.edu. Department of Materials Science and Engineering, Missouri University of Science and Technology, Rolla, Missouri 65409, USA

Thomas W. Heitmann Tel.: +1 573-884-6309 *E-mail address:* heitmannt@missouri.edu. The Missouri Research Reactor, University of Missouri, Columbia, Missouri 65211, USA

1. Introduction:

Zirconium carbide (ZrC_x) ceramics are proposed for use in extreme environments due to a combination of properties including high melting point (3420°C)^[1], high strength (>400 MPa) and hardness (>25 GPA)^[2], high thermal conductivity (>20 W/m·K) and low electrical resistivity (~60 $\mu\Omega$ ·cm)^[3], excellent corrosion resistance^[4,5], and good thermal stability^[6,7]. Some of the applications proposed for ZrC_x ceramics include as a matrix or surface coating for fiber reinforced ultra-high temperature ceramic (UHTC) composites^[8,9], and as structural or fission product barrier coatings for tri-isotropic (TRISO) coated nuclear fuel pellets^[10].

Low cost and high yield methods are needed for the fabrication of powders with controlled composition and microstructure. Various methods have been reported for preparation of ZrC_x. Chemical vapor deposition (CVD) using the reaction between zirconium

halides (e.g. $ZrCl_4$) and hydrocarbon compounds (CH₄) is the most common method for preparing ZrC_x coatings^[11,12]. Bulk ZrC_x ceramics are typically prepared by hot-pressing (HP) or spark plasma sintering (SPS) of ZrC_x powders with or without sintering aids^[13,14]. For powder synthesis, solid state reactions^[15,16,17,18], carbothermal reduction^[19,20], molten salt synthesis^[21], electrochemical synthesis^[22] and laser pyrolysis^[23,24] have been reported.

Solid state reaction and carbothermal reduction have several advantages compared to other synthesis methods including relatively simple processes along with control of the particle morphology of zirconium carbide and carbon stoichiometry. Mechanosynthesis of ZrCx was accomplished by grinding Zr and graphite powders by high-energy milling at room temperature^[25]. Hexagonal monolayer platelets of (111) oriented ZrCx were grown by self-propagating high-temperature synthesis (SHS) using Al as an additive to control growth^[26]. Nanocrystalline ZrCx was produced by reaction of ZrO2, Li2CO3 and Mg in an autoclave at 600°C^[27]. Zirconium oxycarbide powders with carbon stoichiometries ranging from 0.79 to 0.97 were synthesized by carbothermal reduction^[28]. Nanosize particles ZrCx encased by a graphitic shell were synthesized by a combination of mechanical milling and annealing metal-carbon powder mixtures^[29].

Carbothermal reduction is the most common method for synthesis of ZrC_x and has been reported to occur in two steps^[30]. During the first step, ZrO₂ is reduce to oxygen-rich primary zirconium oxycarbide by a solid-gas reaction. The particles formed in the first step are covered by amorphous carbon. In the second step, secondary carbon-rich zirconium oxycarbide forms continuously on the primary zirconium oxycarbide particles. As the reaction proceeds, the two zirconium oxycarbides consume each other, forming a homogeneous composition. At the same time, oxygen is removed from the powders by reaction with the reducing environment that is

rich in carbon monoxide. At the conclusion of the second stage, zirconium carbide powder, with its highest carbon stoichiometry and minimum oxygen content, is produced. Depending on the presence of impurities and the ratios of starting materials, oxygen can be present in different amounts in the zirconium oxycarbide lattice on carbon sites [281]. Unfortunately, many reports of synthesis of ZrCx do not analyze the resulting powders using methods that can unambiguously determine carbon stoichiometry and oxygen content. For example, x-ray diffraction (XRD) analysis is the most common method used to characterize synthesized powders, but the lattice parameter of ZrCx has a complex relationship with carbon and oxygen contents that requires independent measurement of either oxygen or carbon content to explicitly determine carbon stoichiometry and dissolved oxygen content^[31].

The purpose of this study was to investigate the effect of synthesis temperature and the starting ratio of zirconium to carbon on the composition of the resulting ZrC_x powders.

2. Experimental:

2.1 Starting Materials

Commercial ZrH₂ (Min. 95.5%, 27.1 µm, Chemadyne, LLC., Canoga Park, CA) and carbon black (BP-1100, Cabot Corporation, Alpharetta, GA, USA) powders were used as starting materials for ZrC_x synthesis. The powders were batched with molar ratios of ZrH₂:C = 1:0.98 and 1:0.60. The powders were mixed by ball milling using zirconia grinding media in acetone for 12 hours under a rotation speed of 50 rpm. Afterward, rotary evaporation (Rotavapor R-124, Bucchi, Flawil, Germany) was employed to remove the acetone from the slurry at a temperature of 80°C, vacuum of 250 mmHg and a rotation speed of 90 rpm. For synthesis, pellets were produced by uniaxial pressing of three grams of mixed powder.

2.2 Synthesis of ZrCx powders

Synthesis (Reaction 1 and 2, where *y* is the molar ratio of C to Zr in the starting powder and *x* is the ratio of C to Zr in the final ZrC_x) was conducted in a graphite element furnace (3060-FP20, Thermal Technology, Santa Rosa, CA, USA) under flowing argon. The mixed powder was heated from room temperature to 800°C at a heating rate of 10°C/min, and a dwell time of 2 hours to promote decomposition of ZrH₂. Reaction with carbon was promoted by heating to temperatures ranging from 1300°C to 2000°C for 3 hours.

$$ZrH_{2(s)} \to Zr_{(s)} + H_{2(g)}$$
 (1)

$$Zr_{(s)} + yC_{(s)} \to ZrC_{x(s)} + (y - x)C_{(s)}$$
 (2)

2.3 Characterization

Phases were identified using X-ray diffraction (XRD, PANalytical X'Pert3 Powder, Malvern Panalytical Inc., Westborough, MA, USA) with Cu K_{α} radiation ($\lambda = 1.5418 \,\text{Å}$). Lattice parameters and average crystallite sizes were determined using the Rietveld method (RIQAS4, Materials Data Inc., Livermore, CA, USA). The reliability factors R_p and R_{wp} were calculated by Equations 3 and 4:

$$R_p = \frac{\sum_{i \mid cY^{sim}(2\theta_i) - l^{exp}(2\theta_i) + Y^{back}(2\theta_i) \mid}}{\sum_{i \mid l^{exp}(2\theta_i) \mid}}$$
(3)

$$R_{wp} = \left\{ \frac{\left[\sum_{i} w_{i} (cY^{sim}(2\theta_{i}) - I^{exp}(2\theta_{i}) + Y^{back}(2\theta_{i}))^{2}\right]}{\sum_{i} w_{i} (I^{exp}(2\theta_{i}))^{2}} \right\}^{1/2}$$

$$\tag{4}$$

where c is an optimized scaling factor that produces the lowest value of R_{wp} , $w_i = 1/I^{exp}(2\theta_i)$ is a weighting function, $I^{exp}(2\theta_i)$ is the angle-dependent intensity from an experimental spectrum, $Y^{sim}(2\theta_i)$ is the simulated diffraction intensity without the background contribution, $Y^{back}(2\theta_i)$ is the background intensity of the measured pattern^[32]. Total oxygen contents were determined by gas-fusion analysis (Leco, Model TC500, St. Joseph, MI, USA). Transmission electron microscopy (TEM, Tecnai F-20, FEI, Hillsboro, OR, USA) was used to observe the structure of ZrC_x grains using an accelerating voltage of 200 kV. To make TEM specimens, 3 wt% of synthesized powder was suspended in acetone under ultrasonic vibration for 30 minutes, and then dropped on a Cu TEM grid with a carbon film (Carbon Film only on 400 mesh, Copper, Beijing Zhongjingkeyi Technology Co., Ltd, Beijing, China). Selected area electron diffractions (SAED) was used to determine the crystal structures for phase composition analysis. Surface areas were measured by nitrogen absorption (NOVA 1000, Quantachrome, Boynton Beach, FL, USA) and BET analysis. Equivalent particle sizes were calculated by assuming spherical particles using Equation (5),

$$x = 6/S\rho \tag{5}$$

where S is the specific surface area and ρ is the true density of the powder. Neutron powder diffraction (NPD) was measured using a high-resolution powder diffractometer. Neutrons with a wavelength of $\lambda = 1.485$ Å were selected using a double-focusing Si (511) crystal monochromator. About 1.5 grams of powder was loaded into a vanadium cell which was held in an aluminum exchange gas can. Diffraction patterns were collected by a set of five linear position-sensitive detectors (LPSDs). Data was binned in 0.05° steps over the 20° angular

range covered by each LPSD. Five detector arm positions achieved a total 2θ range from 4.45° to 104.4° with position counting for ~ 3.5 hours. Neutron diffraction patterns were analyzed by Rietveld refinement method using an open source code FULLPROF^[33].

3. Results and discussion:

Reaction 1 produced ZrC_x at temperature of 1300°C and higher for both starting ZrH_2 :C ratios. Fig 1a shows the XRD patterns for powders produced using a starting ZrH_2 :C ratio of 1:0.98, but patterns for powders produced from a starting ZrH_2 :C ratio of 1:0.60 were similar (see Appendices). In both cases, ZrC_x , with the $Fm\bar{3}m$ crystal structure (JCPDF card 35-0784), was the only phase detected and no extra peaks were apparent. The peaks shifted to lower angles as the synthesis temperature increased (Fig 1b) indicating that lattice parameters increased with increasing synthesis temperature. Based on the observations described above, ZrC_x can be synthesized by solid state reaction of ZrH_2 and carbon black at temperature as low as 1300°C.

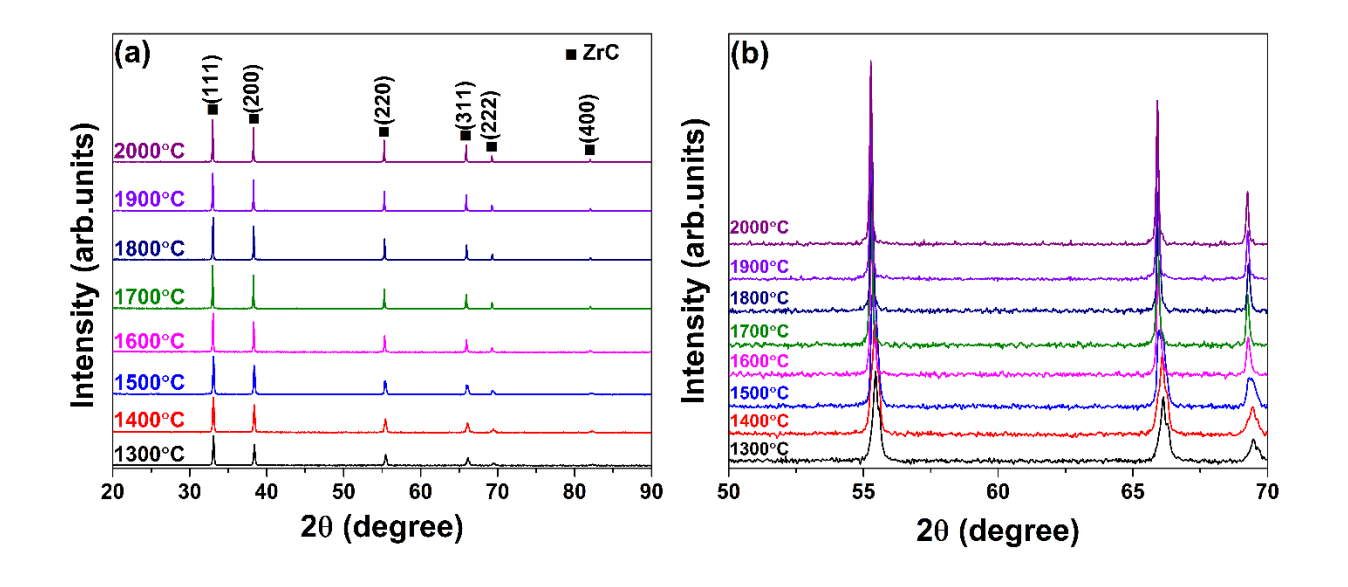


Figure 1. XRD patterns for ZrC_x powders synthesized using a starting ZrH₂:C ratio of 1:0.98 after heating to different temperatures and indexed to the *Fm*3*m* crystal structure showing that:

a) only ZrC_x was detected, and b) peaks shifted to lower angles as synthesis temperature increased.

Amorphous carbon was observed after the powder with a starting ZrH₂:C ratio of 1:0.98 was reacted at 1300°C. Fig 2a shows lighter regions that appear to be amorphous carbon along with darker grains that are ZrC_x. Increasing the synthesis temperature to 2000°C (Fig 2b) caused the excess carbon to disappear. No amorphous carbon was present when the starting ZrH₂:C ratio was 1:0.60 (Figs 2c and 2d). The results indicated that ZrC_x was carbon deficient after synthesis at 1300°C, even with sufficient carbon present to produce fully stoichiometric ZrC_{0.98}. Excess carbon was not detected by XRD analysis for any combination of ZrH₂:C ratio and synthesis temperature. Hence, other reports of ZrC_x synthesis from a starting Zr:C ratio of ~1 likely produce a combination of carbon-deficient ZrC_x and excess amorphous carbon that goes undetected by XRD and other typical characterization methods.

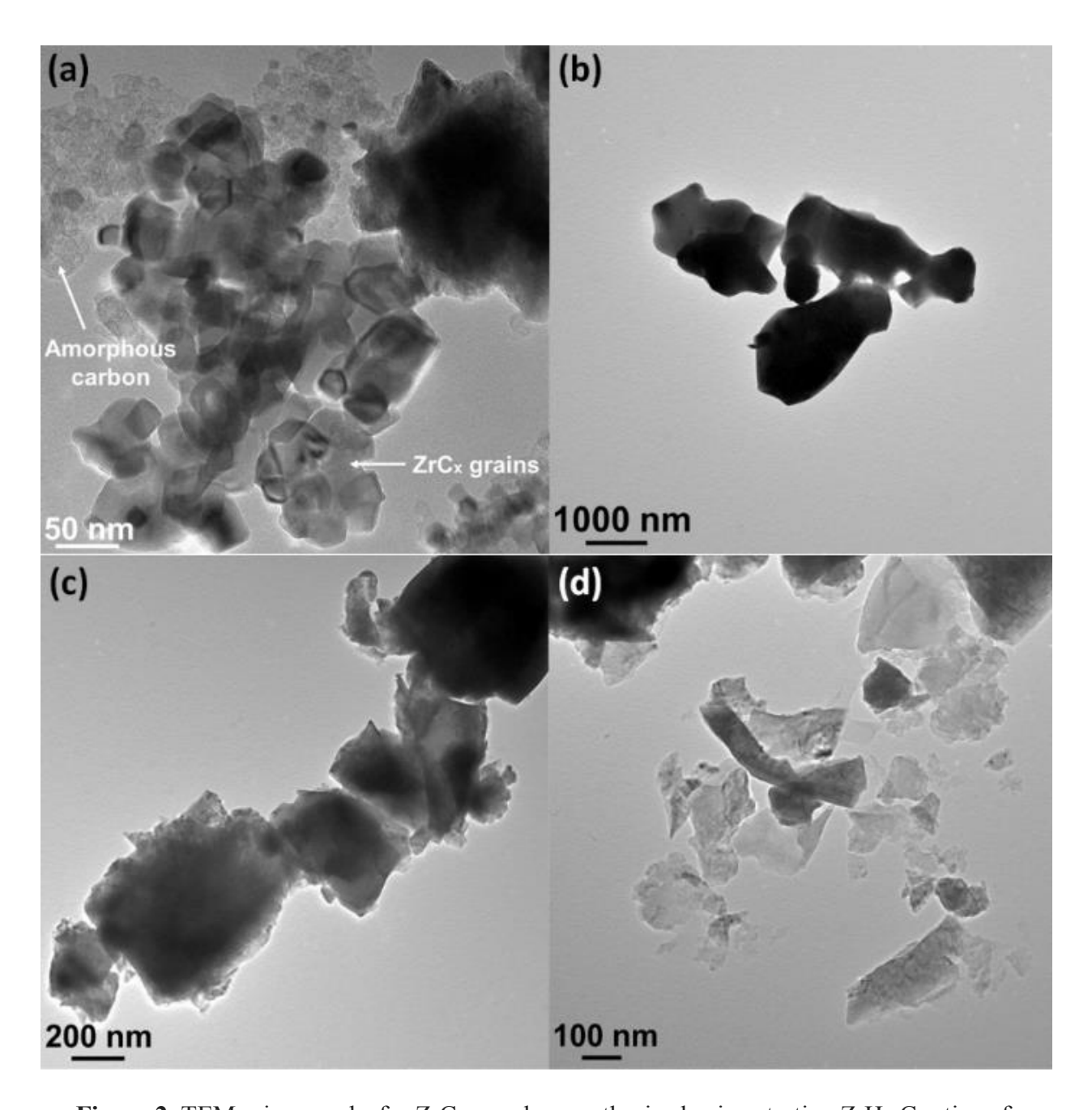


Figure 2. TEM micrographs for ZrC_x powders synthesized using starting ZrH₂:C ratios of: (a)1:0.98 after heating to 1300°C; (b)1:0.98 after heating to 2000°C; (c)1:0.60 after heating to 1300°C; (d)1:0.60 after heating to 2000°C.

The temperature at which excess carbon dissolved into the ZrCx lattice was determined

by heating powder with a starting ZrH₂:C ratio of 1:0.98 to intermediate temperatures between 1300°C and 2000°C. Amorphous carbon was still observed around ZrC_x grains after reaction at 1500°C (Fig 3a). However, no amorphous carbon was found in powders that were heated to 1600°C (Fig 3b). Hence, a synthesis temperature of at least 1600°C was needed to react a majority of the available C with Zr for the powder produced with a starting ZrH₂:C ratio of 1:0.98.

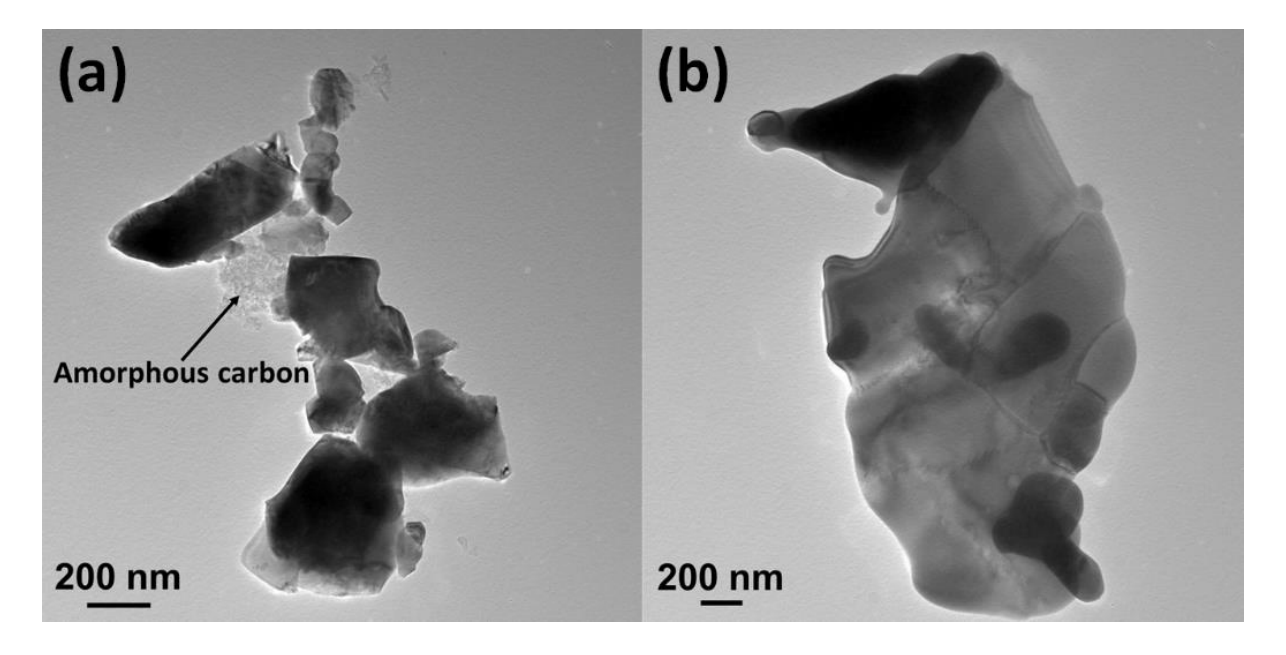


Figure 3. TEM micrographs for ZrC_x powders synthesized using a starting ZrH₂: C ratio of 1: 0.98 after heating to (a) 1500°C, (b) 1600°C.

The synthesis temperature affected the lattice parameter of ZrC_x powders. As can be seen in Fig 4, the lattice parameter of powders synthesized at temperatures below 1500°C increased with increasing synthesis temperature from 4.686 Å for synthesis at 1300°C to 4.699 Å for synthesis at 1500°C (see Appendices). The increase in lattice parameter could be due to the increasing carbon content in the ZrC_x lattice in this temperature range based on the relationship

reported by Jackson and Lee^[34]. In contrast, the lattice parameter decreased in the next temperature regime from 4.699 Å at 1500°C to 4.694 Å 1700°C. In this regime, the decrease in lattice parameter was attributed to the loss of dissolved oxygen and/or nitrogen from the ZrC_x lattice^[35]. The oxygen and nitrogen impurities could come from the starting ZrH₂ powder, which contains 0.47 wt% oxygen, as measured by the gas fusion method, or the flowing argon gas used during synthesis, which contained a few parts per million of both oxygen and nitrogen impurities. At 1700°C and above, the lattice parameter was constant at ~4.694 Å, indicating that neither the carbon stoichiometry nor the dissolved content of oxygen and/or nitrogen changed significantly in this temperature regime.

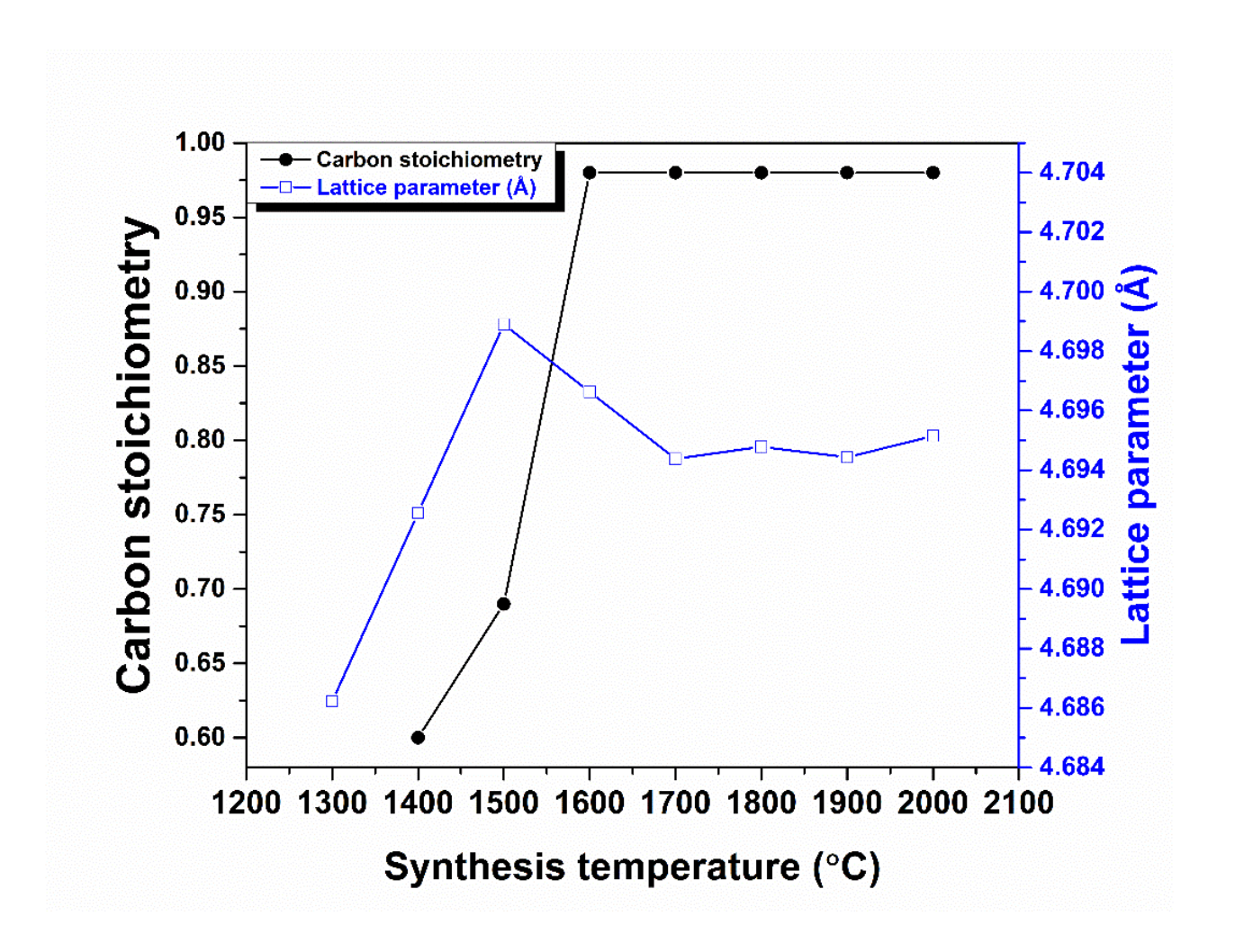


Figure 4. Lattice parameter and estimated carbon stoichiometry for ZrC_x powders synthesized using a starting ZrH₂:C ratio of 1:0.98 that were heated to different temperatures. Note that error bars on the lattice parameters are smaller than the data points. The lines were added as guides.

Changes in the lattice parameter indicated that the carbon content of ZrC_x changed as synthesis temperature changed for powders synthesized using a starting ZrH₂:C ratio of 1:0.98. The correlation between lattice parameter and carbon content determined by Jackson and Lee^[34] was used to estimate carbon content from lattice parameters determined by Rietveld refinement of XRD patterns. The lattice parameter after synthesis at 1300°C was ~4.686 Å, which would indicate a carbon content of less than ZrC_{0.60} after reaction at this temperature. Since the minimum C content shown by most Zr-C phase diagrams is $x = 0.60^{[36]}$, the lattice parameter for this synthesis condition may have been affected by dissolved oxygen and/or nitrogen or by strain that was due to the fine crystallite size (discussed below). Hence, no estimate of carbon stoichiometry was made for powders synthesized at 1300°C by this method. The lattice parameter was 4.693Å after synthesis at 1400°C, which correlated to a carbon stoichiometry of ZrC_{0.60}. Likewise, the lattice parameter increased to 4.699 Å after synthesis at 1500°C, indicating a carbon stoichiometry of ZrC_{0.69}. At temperatures of 1600°C and higher, full carbon stoichiometry was assumed based on TEM observations discussed above wherein no excess carbon was present. Lattice parameters of those powders are in the range of 4.694 Å to 4.697 Å (see Appendices), which is slightly lower than the value of ~4.697 Å indicated by Jackson and Lee^[34] for ZrC_{0.98}. The reduction in lattice parameter compared to the fully stoichiometric value could be due to either a small fraction of carbon vacancies or residual dissolved oxygen and/or nitrogen in the lattice.

Crystallite size increased as synthesis temperature increased. As shown in Fig 5 for a starting ZrH₂:C ratio of 1:0.98, synthesis at low temperatures (1300°C and 1400°C) resulted in a crystallite size between 40 nm and 50 nm. At this size, the particles could have significant compressive strain, which could also affect the lattice parameter measurements. Rietveld refinement indicated residual strains of up to about 0.09% after synthesis at 1300°C (Table 1). Above 1400°C, crystallite size increased continuously with increasing synthesis temperature, reaching ~130 nm for a synthesis temperature of 2000°C. Representative morphologies of assynthesized ZrC_x powders were shown in Figs 2 and 3. For powders synthesized at temperatures of 1500°C and higher, crystallite sizes estimated by Rietveld method were smaller than observed by TEM. For example, Fig 6 shows a TEM micrograph for powder synthesized at 1600°C. Some of the crystallites appeared to be smaller than 100 nm, which is consistent with the size determined by Rietveld refinement of XRD data. However, most of the crystallites were larger than 200 nm. The apparent differences in crystallite size between values estimated from XRD and TEM may be due to the limited number of particles observed by TEM, the different shapes of the crystals (i.e., not spherical), or the crystallite size distribution.

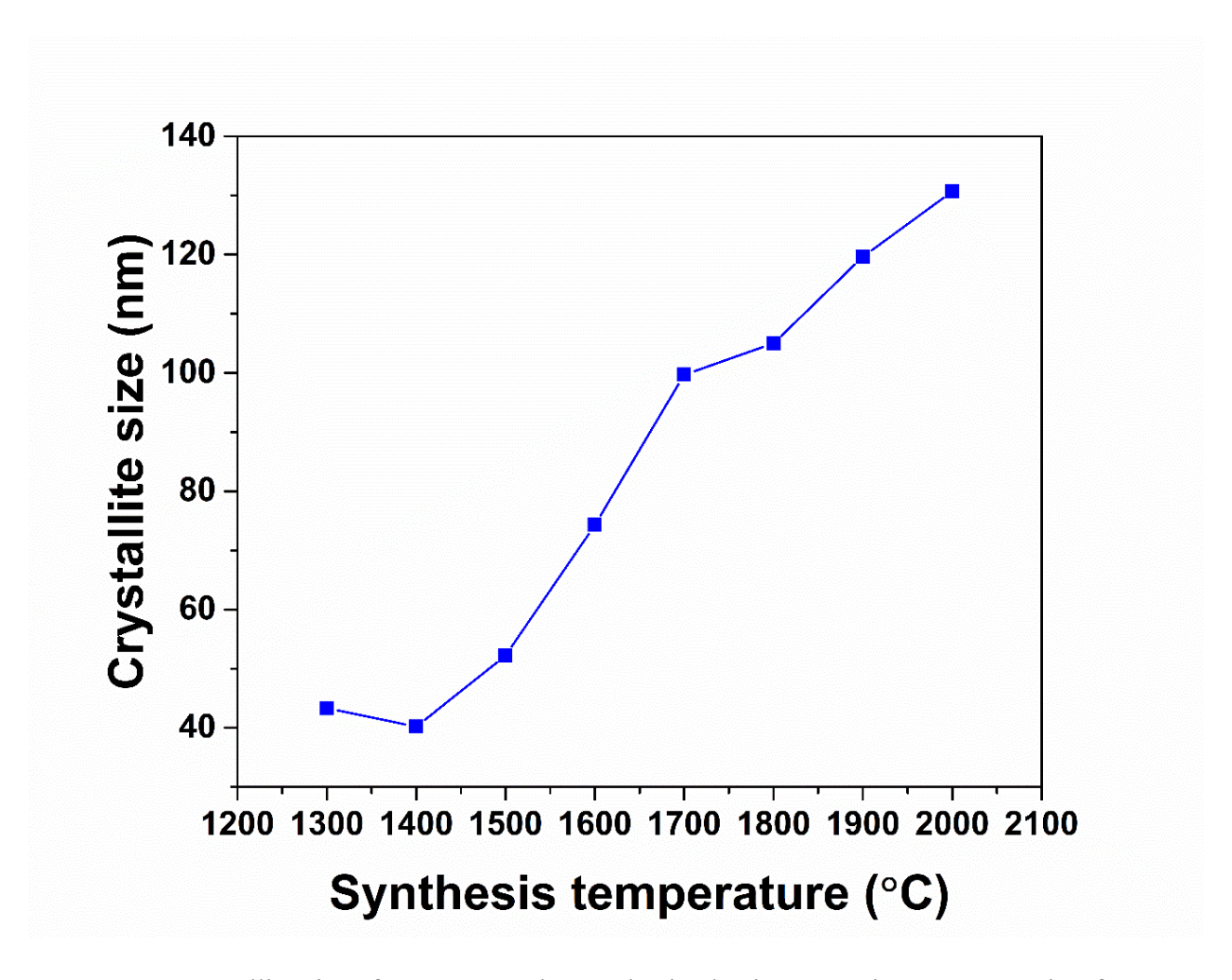


Figure 5. Crystallite sizes for ZrC_x powder synthesized using a starting ZrH₂:C ratio of 1:0.98 heated to different temperatures.

Synthesis temperature			
(°C)		1300	2000
Starting ZrH2:C ratio			
1:0.6	R _p (%)	5.77	5.28
	R _{wp} (%)	4.98	4.77
	Lattice parameter(Å)	4.679	4.678
	Strain	2.50×10^{-4}	2.50×10^{-5}
	Carbon stoichiometry	0.6	0.6
	Crystallite size (nm)	81.6	108.0
	Surface area m ² /g	0.795	0.636
	Particle size (µm)	1.138	1.422
	Oxygen content (wt%)	1.953	2.297
	C occupancy	0.60	0.60
	O and N occupancy	0.14	0.12
1:0.98	R _p (%)	5.33	7.63
	R _{wp} (%)	5.07	5.28
	Lattice parameter(Å)	4.682	4.695
	Strain	8.50×10^{-4}	1.25×10^{-4}
	Carbon stoichiometry	N/A	0.98
	Crystallite size (nm)	43.3	130.7
	Surface area m ² /g	5.310	0.612
	Particle size (µm)	0.170	1.478
	Oxygen content (wt%)	1.997	1.011
	C site occupancy	0.82	0.98

Table 1. Reliability factors of Rietveld refinement, lattice parameters, estimated carbon stoichiometry, crystallite sizes, surface areas, particle sizes, oxygen contents and C and O occupancies of ZrC_x powders mixed using starting ZrH₂:C ratio of 1:0.6 and 1:0.98 and synthesized at 1300°C and 2000°C.

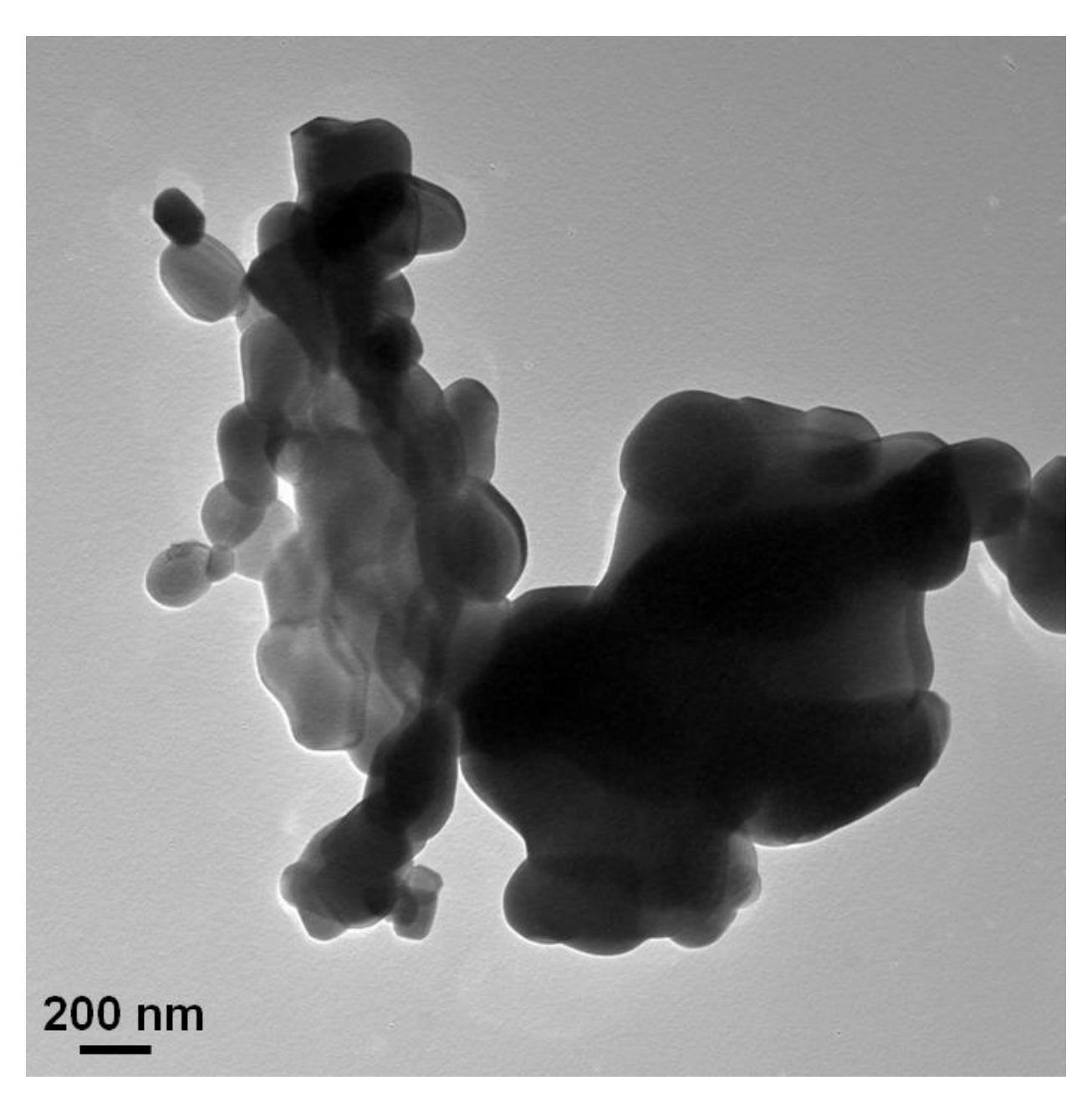


Figure 6. TEM micrographs for ZrC_x powders synthesized using a starting ZrH_2 : C ratio of 1: 0.98 after heating to 1600°C.

All of the synthesized powders contained oxygen impurities. Oxygen contents determined by gas fusion ranged from as high as 2.3 wt% for powder synthesized at 2000°C for a starting ZrH₂:C ratio of 1:0.60 to as low as 1.0 wt% for powder synthesized at 2000°C using a starting

ZrH₂:C ratio of 1:0.98 (Table 1). High resolution TEM revealed that particles all had an exterior oxide layer that was typically about 5 nm thick that accounted for at least some of the measured oxygen content (Fig 7). However, oxygen can also dissolve into the lattice and occupy carbon sites that would otherwise be vacant, so some of the measured oxygen content could be dissolved in the lattice. Likewise, nitrogen can dissolve into the lattice and occupy carbon vacancies. Unfortunately, gas fusion analysis determines only total oxygen and nitrogen contents cannot distinguish between surface impurities and those on lattice sites. Based on this analysis, oxygen contents appear to decrease as carbon stoichiometry increases. The presence of dissolved oxygen also complicates determination of carbon stoichiometry from the lattice parameter of ZrC_x since dissolved oxygen leads to a decrease in lattice parameter compared to full occupancy of carbon lattice sites by carbon, but an increase in lattice parameter compared to the presence of vacancies.

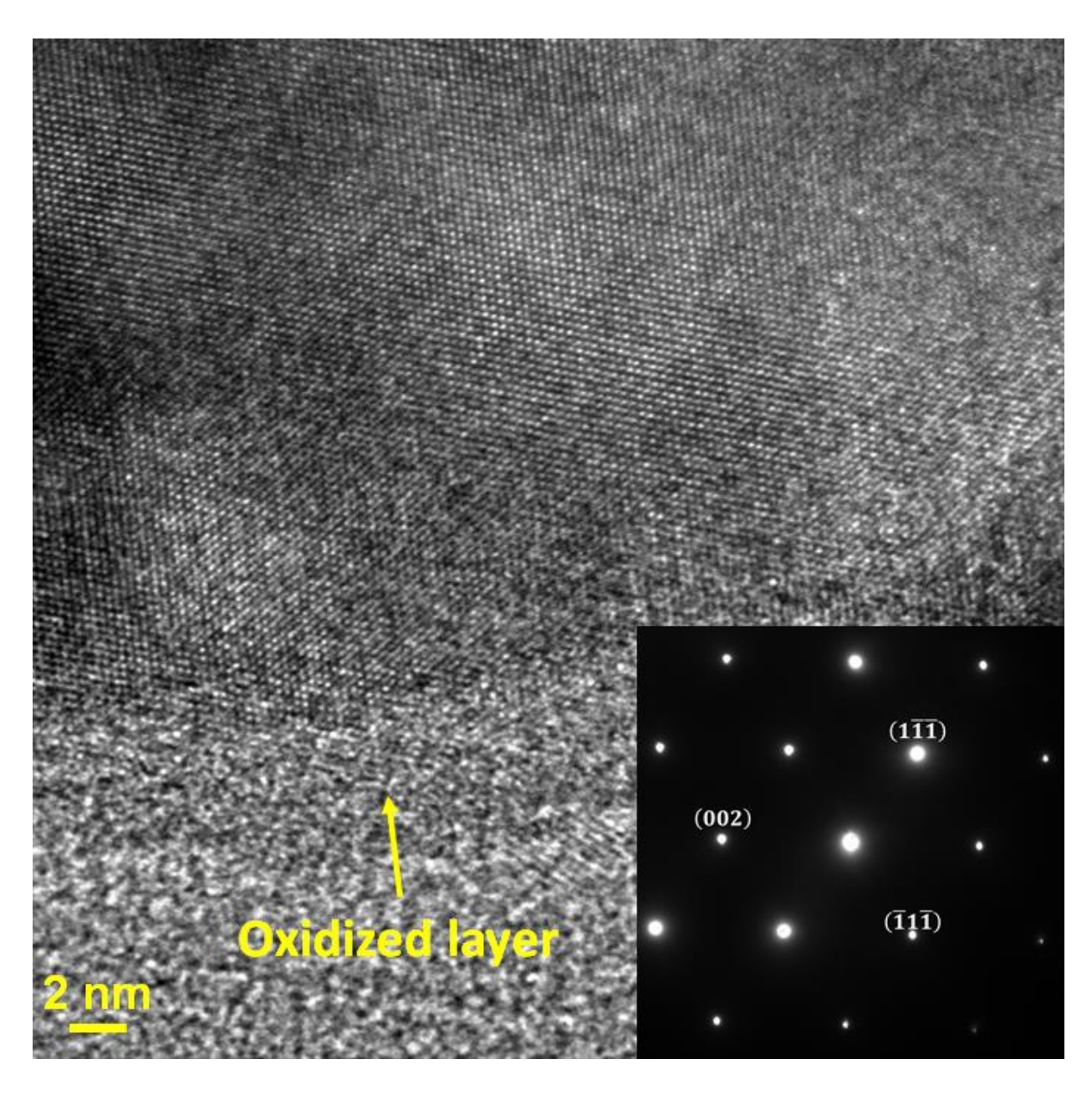


Figure 7. High resolution TEM micrographs of a ZrC_x particle synthesized using a starting ZrH_2 :C ratio of 1:0.98 after heating to 2000°C and an inset SAED pattern indexed to the $Fm\overline{3}m$ crystal structure.

Characterization methods typically used in studies of ZrC_x synthesis are not able to unambiguously determine the fraction of vacant carbon sites or the number of lattice sites

occupied by oxygen and/or nitrogen due to lack of sensitivity or convoluted effects^[35,37]. For example, XRD patterns are dominated by scattering from the Zr sub-lattice due to its much higher x-ray scattering factor for Zr (40) compared to carbon (6), nitrogen (7), oxygen (8), or carbon vacancies (0). As a result, analysis of peak intensity from XRD patterns does not provide enough information to independently determine carbon, oxygen, and nitrogen contents or site occupancies. In contrast, the neutron scattering factors for C (5.6 barn) and N (11.5 barn), and oxygen (4.3 barn) are comparable to those of Zr (6.5 barn), which enables more accurate refinement of peak intensity data and more reliable estimation of site occupancies from neutron powder diffraction patterns than is possible from XRD. Fig 8 shows neutron diffraction patterns for ZrC_x powders synthesized using a starting ZrH₂:C ratio of 1:0.98 and heated to 1300°C and 2000°C. As with the XRD patterns, all of the peaks in both patterns were indexed to ZrC_x with the $Fm\bar{3}m$ crystal structure (JCPDF card 35-0784). Rietveld refinement was used to estimate the fraction of C sites occupied (Table 1). For this analysis, C sites were considered to either be occupied (i.e., contain a C, O, or N atom) or vacant without attempting to refine for each individual atom type. This analysis estimated that the fraction of C sites occupied after synthesis at 1300°C was 0.82. Increasing the synthesis temperature to 2000°C increased the C site occupancy to 0.98, which is consistent with observations by TEM that all of the initial carbon had been dissolved into the lattice (Fig 2b) as mentioned above. Based on this analysis and accepted Zr-C phase diagrams, full carbon stoichiometry was reached (i.e., ZrC_{0.98} was formed). ZrC_x synthesized using a starting ZrH₂:C ratio of 1:0.6 showed that the fraction of carbon sites occupied was about 0.60 regardless of the synthesis temperature (Table 1). All of the analysis performed as part of the present study indicates that neutron diffraction is a reliable method for determining occupancy of carbon sites in the ZrC_x lattice.

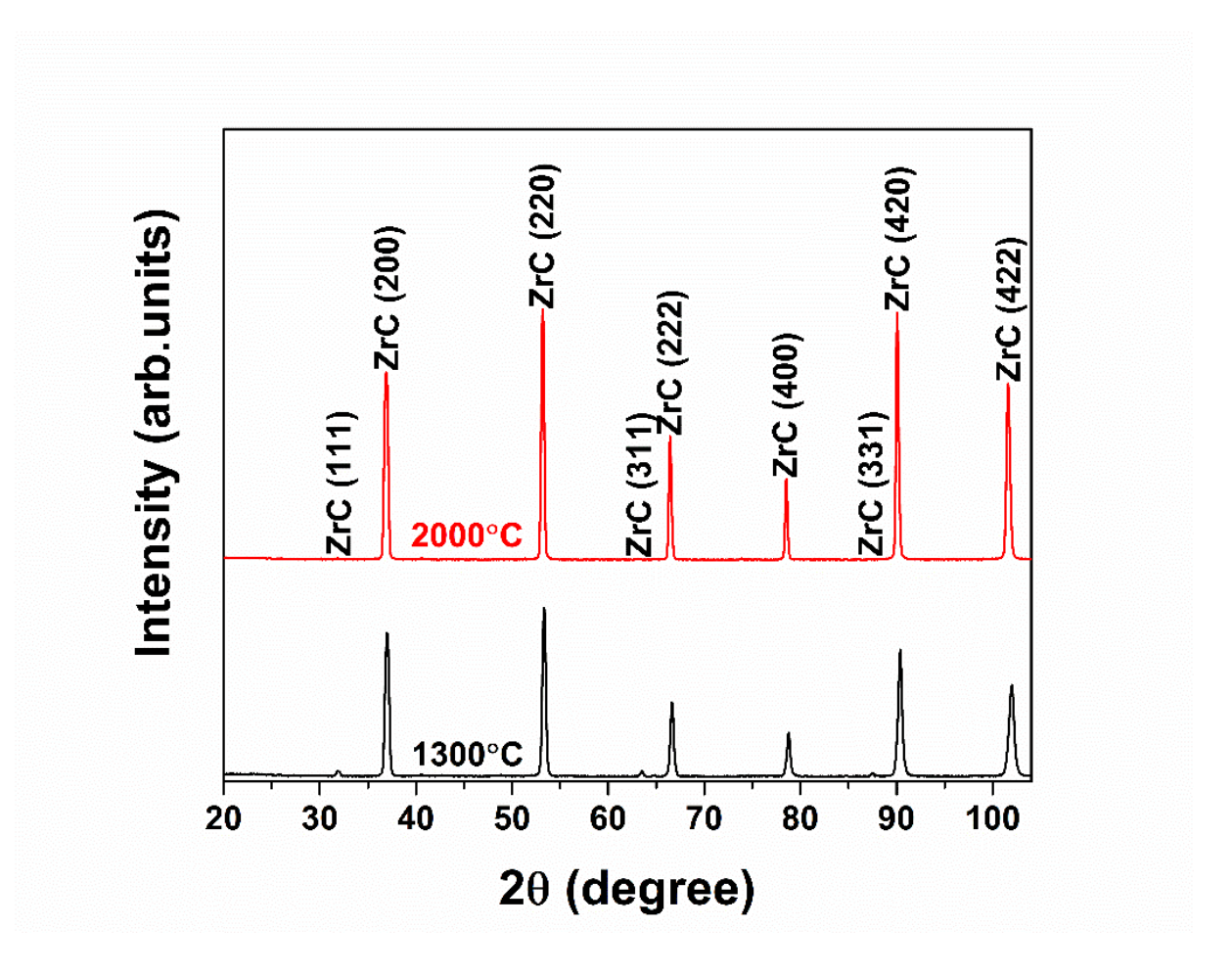


Figure 8. Neutron powder diffraction patterns for ZrC_x powder synthesized using a starting ZrH₂:C ratio of 1:0.98 after heating to 1300°C and 2000°C.

4. Conclusions:

Solid state reactions of ZrH₂ and carbon black were used to synthesize ZrC_x powders. Different ratios of the reactants and different reaction temperatures were used to study their effects on particle size and carbon stoichiometry. Single phase ZrC_x was synthesized at temperatures as low as 1300°C. Below 1600°C, carbon was not fully incorporated into the ZrC_x lattice. Observations by TEM indicated that all of the available carbon reacted with ZrH₂ at

1600°C and higher. Increasing the synthesis temperature increased the size of the resulting ZrC_x crystallites from ~40 nm after reaction at 1300°C or 1400°C to ~130 nm after reaction at 2000°C. Oxygen impurities were present in all of the powders regardless of the starting ZrH₂:C ratio. Some of the oxygen was present as an oxide layer on the exterior of ZrC_x particles, while the rest of the oxygen impurities were dissolved in the ZrC_x lattice. Although XRD can confirm formation of the rock salt carbide structure, it was not able to determine carbon stoichiometry or dissolved oxygen content in transition metal carbides. Neutron diffraction was able to discern differences in site occupancy, showing that carbon stoichiometry increased and dissolved oxygen content decreased with increasing synthesis temperature.

Acknowledgements:

This research was supported by the Ceramics program of the U.S. National Science Foundation as part of project DMR 1742086. The neutron powder diffraction measurements were made at The Missouri Research Reactor, University of Missouri (MURR).

References:

- [1] Sara RV. The system zirconium—carbon. J Amer Ceramic Soc. 1965;48(5):243-247.
 https://doi.org/10.1111/j.1151-2916.1965.tb14729.x.
- ^[2] Pierson HO. Handbook of refractory carbides and nitrides: properties, characteristics, processing and applications. Norwich, NY: William Andrew; 1996.
- [3] Grossman LN. High-Temperature Thermophysical Properties of Zirconium Carbide. J Amer Ceramic Soc. 1965;48(5):236-242. https://doi.org/10.1111/j.1151-2916.1965.tb14728.x.
- [4] Katoh Y, Vasudevamurthy G, Nozawa T, Snead LL. Properties of zirconium carbide for nuclear fuel applications. J Nuclear Materials. 2013;441(1-3):718-742. https://doi.org/10.1016/j.jnucmat.2013.05.037.
- [5] Shen X, Li K, Li H, Du H, Cao W, Lan F. Microstructure and ablation properties of zirconium carbide doped carbon/carbon composites. Carbon. 2010;48(2):344-351. https://doi.org/10.1016/j.carbon.2009.09.035.
- [6] Taylor RE. Thermal conductivity of zirconium carbide at high temperatures. J Amer Ceramic Soc. 1962;45(7):353-354. https://doi.org/10.1111/j.1151-2916.1962.tb11166.x.
- [7] Taylor RE, Morreale J. Thermal conductivity of titanium carbide, zirconium carbide, and titanium nitride at high temperatures. J Amer Ceramic Soc. 1964;47(2):69-73. https://doi.org/10.1111/j.1151-2916.1964.tb15657.x.
- [8] Zhao D, Zhang C, Hu H, Zhang Y. Preparation and characterization of three-dimensional carbon fiber reinforced zirconium carbide composite by precursor infiltration and pyrolysis process. Ceramics International. 2011;37(7):2089-2093.

 https://doi.org/10.1016/j.ceramint.2011.02.024.

- ^[9] Zhu Y, Wang S, Li W, Zhang S, Chen Z. Preparation of carbon fiber-reinforced zirconium carbide matrix composites by reactive melt infiltration at relative low temperature. Scripta Materialia. 2012;67(10):822-825. https://doi.org/10.1016/j.scriptamat.2012.07.044.
- [10] Sabharwall P, Bragg-Sitton SM, Stoots C. Challenges in the development of high temperature reactors. Energy Conversion Mgmt. 2013;74:574-581.
 https://doi.org/10.1016/j.enconman.2013.02.021.
- [11] Wang Y, Liu Q, Liu J, Zhang L, Cheng L. Deposition mechanism for chemical vapor deposition of zirconium carbide coatings. J Amer Ceramic Soc. 2008;91(4):1249-1252. https://doi.org/10.1111/j.1551-2916.2007.02253.x.
- [12] Liu Q, Zhang L, Cheng L, Wang Y. Morphologies and growth mechanisms of zirconium carbide films by chemical vapor deposition. J Coatings Tech Res. 2009;6(2):269-273. https://doi.org/10.1007/s11998-008-9117-5.
- [13] Barnier P, Brodhag C, Thevenot F. Hot-pressing kinetics of zirconium carbide. J Materials Science. 1986;21(7):2547-2552. https://doi.org/10.1007/BF01114305.
- [14] Wei X, Back C, Izhvanov O, Haines CD, Olevsky EA. Zirconium carbide produced by spark plasma sintering and hot pressing: Densification kinetics, grain growth, and thermal properties. Materials. 2016;9(7):577. 10.3390/ma9070577.
- [15] Tsuchida T, Kawaguchi M, Kodaira K. Synthesis of ZrC and ZrN in air from mechanically activated Zr-C powder mixtures. Solid State Ionics. 1997;101:149-154. https://doi.org/10.1016/S0167-2738(97)84023-4.
- [16] Yen BK. X-ray diffraction study of mechanochemical synthesis and formation mechanisms of zirconium carbide and zirconium silicides. J Alloys Compounds. 1998;268:(1-2):266-269. https://doi.org/10.1016/S0925-8388(97)00581-1.

- [17] Tsuchida T, Yamamoto S. Mechanical activation assisted self-propagating high-temperature synthesis of ZrC and ZrB2 in air from Zr/B/C powder mixtures. J Euro Ceramic Society. 2004;24(1):45-51. https://doi.org/10.1016/S0955-2219(03)00120-1.
- [18] Song MS, Huang B, Zhang MX, Li JG. Formation and growth mechanism of ZrC hexagonal platelets synthesized by self-propagating reaction. J Crystal Growth. 2008;310(18):4290-4294. https://doi.org/10.1016/j.jcrysgro.2008.07.016.
- [19] Sacks MD, Wang CA, Yang Z, Jain A. Carbothermal reduction synthesis of nanocrystalline zirconium carbide and hafnium carbide powders using solution-derived precursors. J Materials Science 2004;39(19):6057-6066.
 https://doi.org/10.1023/B:JMSC.0000041702.76858.a7.
- [20] Dolle M, Gosset D, Bogicevic C, Karolak F, Simeone D, Baldinozzi G. Synthesis of nanosized zirconium carbide by a sol–gel route. J Euro Ceramic Society. 2007;27(4):2061-2067. https://doi.org/10.1016/j.jeurceramsoc.2006.06.005.
- [21] Ding J, Guo D, Deng C, Zhu H, Yu C. Low-temperature synthesis of nanocrystalline ZrC coatings on flake graphite by molten salts. Applied Surface Science. 2017;407:315-321.
 https://doi.org/10.1016/j.apsusc.2017.02.196.
- [22] Dai L, Wang X, Zhou H, Yu Y, Zhu J, Li Y et al. Direct electrochemical synthesis of zirconium carbide from zirconia/C precursors in molten calcium chloride. Ceramics International. 2015;41(3):4182-4188. https://doi.org/10.1016/j.ceramint.2014.12.101.
- [23] Leconte Y, Maskrot H, Combemale L, Herlin-Boime N, Reynaud C. Application of the laser pyrolysis to the synthesis of SiC, TiC and ZrC pre-ceramics nanopowders. J Anal Appl Pyrolysis. 2007;79(1-2):465-470. https://doi.org/10.1016/j.jaap.2006.11.009.

- ^[24] Combemale L ,Leconte Y, Portier X, Herlin-Boime N, Reynaud C. Synthesis of nanosized zirconium carbide by laser pyrolysis route. J Alloys Compounds. 2009;483(1-2):468-472. https://doi.org/10.1016/j.jallcom.2008.07.159.
- [25] Matteazzi P, Le Caër G. Room-Temperature Mechanosynthesis of Carbides by Grinding of Elemental Powders. J Amer Ceramic Soc. 1991;74(6):1382-1390.

 https://doi.org/10.1111/j.1151-2916.1991.tb04116.x.
- [26] Song M, Huang B, Zhang M, Li J. Formation and growth mechanism of ZrC hexagonal platelets synthesized by self-propagating reaction. J Crystal Growth. 2008;310(18):4290-4294. https://doi.org/10.1016/j.jcrysgro.2008.07.016.
- [27] Wang L, Si L, Zhu Y, Qian Y. Solid-state reaction synthesis of ZrC from zirconium oxide at low temperature. Int J Refract Met H. 2013;38:134-136.
 https://doi.org/10.1016/j.ijrmhm.2012.12.001.
- [28] Gendre M, Maître A, Trolliard G. Synthesis of zirconium oxycarbide (ZrCxOy) powders: Influence of stoichiometry on densification kinetics during spark plasma sintering and on mechanical properties. J Euro Ceramic Society. 2011;31(13):2377-2385. https://doi.org/10.1016/j.jeurceramsoc.2011.05.037.
- [29] Bokhonov BB, Dudina DV. Synthesis of ZrC and HfC nanoparticles encapsulated in graphitic shells from mechanically milled Zr-C and Hf-C powder mixtures. Ceramics International. 2017;43(16):14529-14532. https://doi.org/10.1016/j.ceramint.2017.07.164.
- David J, Trolliard G, Gendre M. TEM study of the reaction mechanisms involved in the carbothermal reduction of zirconia. J Euro Ceramic Society. 2013;33(1):165-179. https://doi.org/10.1016/j.jeurceramsoc.2012.07.024.

- [31] Mitrokhin VA, Lyutikov RA, Yurkova RS. Change in the lattice constant of zirconium carbide in the region of homogeneity. Inorg. Mater. 1975;11(6):978-980.
- [32] Vitalij KP, Peter YZ. Fundamentals of Powder Diffraction and Structural Characterization of Materials. 2nded. New York, NY: Springer; 2009.
- [33] J. Rodriguez-Carvajal, FULLPROF version July-2017, ILL.
- [34] Jackson HF, Lee WE. Properties and characteristics of ZrC. In: Konings RJM, eds. Volume 2 in Comprehensive Nuclear Materials. Amsterdam, Netherland: Elsevier; 2012:339-372.
- [35] Harrison RW, Lee WE. Processing and properties of ZrC, ZrN and ZrCN ceramics: a review. Adv in Applied Ceramics. 2016;115(5):294-307. https://doi.org/10.1179/1743676115Y.0000000061.
- [36] Diagram 8963 in Phase Diagrams for Ceramists Volume X: Borides, Carbides, and Nitrides.

 McHale AE ed. Westerville, OH: American Ceramic Society. 1994.
- [37] Sarkar SK, Miller AD, Mueller JI. Solubility of oxygen in ZrC. J Amer Ceramic Soc. 1972;55(12):628-630. https://doi.org/10.1111/j.1151-2916.1972.tb13457.x.